FATIGUE LIFE ANALYSIS FOR THE CLEANING SIEVE BOX OF A COMBINE HARVESTER BASED ON MEASURED LOADS

基于实测载荷的联合收获机清选筛箱疲劳寿命分析

Yu PAN, Zheng MA*), Shuai WANG, Zhiping WU, Yongle ZHU, Yaoming LI School of Agriculture Engineering, Jiangsu University, Zhenjiang 212013, China Tel: 18796087291; E-mail: mazheng123@ujs.edu.cn

DOI: https://doi.org/10.35633/inmateh-77-14

Keywords: combine harvester; cleaning sieve box; fatigue life; finite element analysis; life prediction

ABSTRACT

The cleaning sieve box is a key component to achieve the cleaning of a combine harvester, and its service life directly affects the reliability of the entire machine. Aiming at the high quality of the cleaning sieve box and the cyclic loading during operation (which can easily cause fatigue damage and affect its service life), a fatigue durability analysis method for the cleaning sieve box based on a test bench is proposed. First, the deformation and stress distribution of the sieve box are analyzed through modal and dynamic simulation to identify the hotspots of fatigue damage in the sieve box. On this basis, a sieve box test bench was designed and built to collect load signals of the sieve box. The layout of sensor measuring points was optimized based on simulation results and the force characteristics of the sieve box was analyzed through signal processing. Then based on the load signals from multiple measuring points, a fatigue load spectrum was developed using nCode software, and the fatigue life of the sieve box was predicted using Miner's fatigue damage theory. The results indicated that there are multiple stress concentration areas in the connection area between the shaking plate, fish scale screen and the side wall of the screen frame of the sieve box, which are the fatigue damage risk areas. The stress value in the connection area of the tail screen is the highest. Overall, the fatigue life of the front half of the sieve box is generally higher than that of the rear half. The connection area between the side walls of the screen frame and the tail screen is the weak fatigue durability area, with fatigue lives of 5.829 × 106 and 5.591 × 106 cycles, respectively. This study provides a certain basis for the design and optimization of the cleaning sieve box structure.

摘要

清选筛箱是实现联合收获机清选功能的关键部件,其使用寿命直接影响整机可靠性。针对清选筛箱质量大,工作时承受往复周期性载荷,易造成疲劳损伤且影响使用寿命,本文提出一种基于试验台架的清选筛箱疲劳耐久分析方法。首先,通过模态和动力学仿真,分析筛箱的变形、应力分布情况,识别筛箱疲劳损伤热点区域。在此基础上,设计并搭建筛箱试验台架以采集筛箱载荷信号,基于仿真结果优化传感器测点布置,并通过信号处理分析筛箱受力特性。结合多测点载荷信号,采用 nCode 软件编制疲劳载荷谱,并基于 Miner 疲劳损伤理论,对筛箱疲劳寿命进行预测。研究结果表明,筛箱内部抖动板、鱼鳞筛等零部件与筛框侧壁连接区域出现多处应力集中区域,为其结构的疲劳损伤危险区域,其中尾筛连接区域应力值最大。整体而言,筛箱前半部分的疲劳寿命普遍高于后半部分,筛框两侧侧壁与尾筛的连接区域为筛箱结构中疲劳耐久薄弱区域,其疲劳寿命分别为5.829×106、5.591×106循环次数。该研究为清选筛箱结构设计和优化提供了一定参考依据。

INTRODUCTION

The combine harvester is an important equipment in agricultural mechanization, which can achieve various operations such as crop harvesting, threshing, cleaning and bundling, improving the efficiency and quality of agricultural production (*Doungpueng et al., 2020; Yang et al., 2024*). The cleaning sieve box is the core component of the combine harvester cleaning system, which has large mass and complex structure, and is in a reciprocating motion state for a long-time during operation. Most of cleaning sieve boxes on the market mainly rely on prototype field experiments for structural optimization, lacking systematic structural design and performance evaluation methods.

Yu Pan (Master's Student); Zheng Ma (Professor); Shuai Wang (Lecturer); Zhiping Wu (Ph.D. Candidate); Yongle Zhu (Ph.D. Candidate); Yaoming Li (Professor)

Combine harvesters often face complex working conditions such as uneven terrain, tilting of the machine, and overall vibration in practical operations, which cause the cleaning sieve box bearing multiple loads and easily lead to structural failures such as bearing fracture and screen deformation. This not only shortens the service life of the sieve box, but also has a negative impact on the overall efficiency of the machine (*Linhares et al., 2024*). With the continuous increase in the feeding amount of the grain combine harvester, the load borne by the cleaning sieve box continues to increase, and higher requirements have been put forward for its operational performance and fatigue life (*Mirzazadeh et al., 2022; Jin et al., 2022*).

Ramatsetse et al (2017) used finite element analysis to evaluate the structural performance of vibrating screens. Through dynamic analysis and modal testing, weak parts of the screen structure were identified for targeted optimization design, improving the overall performance and service life of the equipment. Rumiche et al (2021) conducted metallurgical failure analysis on the welded transmission beam of the vibrating screen. Using macroscopic analysis, and hardness testing, combined with fatigue design criteria, the influence of the transmission beam weld on the fatigue strength of the vibrating screen was evaluated. Linhares and Vimieiro (2024) investigated the influence of processing errors in the drive shaft of the vibrating screen on its operation and vibration parameters. They found that even small minor processing errors of the eccentric block or premature wear of the keyway and shaft would cause distortion in the vibration trajectory of the equipment, thereby leading to structural failure (such as cracks and component fractures) and performance degradation.

Pang et al (2023) focused on the vibration problem caused by rotor system imbalance during the operation of the grain cleaning sieve box. They tested the vibration characteristics of the cleaning sieve box and conducted structural optimization to reduce unbalanced vibration of the system. Li et al (2019) used the method of calculating the excitation force through the classical transmission path to analyze the time-frequency domain of the vibration signal of the cleaning sieve box. Based on the abnormal amplitude of the excitation force, they identified the manufacturing defects of the cleaning sieve. Taking the cleaning device of a grain combine harvester as the object, Wang et al (2019) established a dynamic model of the cleaning sieve. They studied the factors affecting the fatigue life of the cleaning device and obtained the key factors affecting the fatigue life of the main components of the cleaning device. Current researches on the cleaning sieve boxes of combine harvesters mainly focus on optimizing their working performance. Most of them use numerical simulation and bench testing methods to analyze their vibration characteristics and other performance indicators. However, regarding the fatigue durability of sieve box structures, it is relatively scarce.

The fatigue durability of the cleaning sieve box of a mainstream tracked combine harvester was analyzed. First, a finite element simulation model of the cleaning sieve box was established to obtain the stress distribution of the sieve box and identify the hotspot areas of fatigue damage in the sieve box. In this way, a layout plan for the strain sensor was developed. Then a test bench for the cleaning sieve box was built for dynamic test according to the actual working conditions. The strain load signals from each measuring point of the cleaning sieve box were collected to prepare load spectra and analyze the fatigue life of the sieve box to determine weak fatigue durability areas in the sieve box structure.

MATERIALS AND METHODS

Composition of the cleaning sieve box

The eccentric wheel sliding block cleaning sieve box that is widely used in tracked full feed grain harvesters is taken as an example. This sieve box is mainly composed of shaking plate, sieve frame, fish scale screen, tail screen, mesh screen, and driving part. Its structure is shown in Fig. 1. The cleaning sieve box has a length of 2.1 m, a width of 0.91 m, and a weight of about 80 kg.

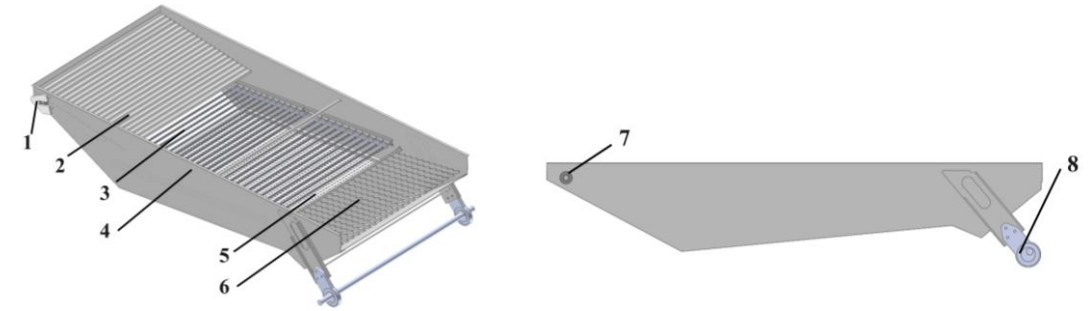


Fig. 1 - Structure of the cleaning sieve box

1. Guide rail; 2. Shaking plate; 3. Fish scale screen; 4. Sieve frame; 5. Mesh screen; 6. Tail screen; 7. Front guide rail; 8. Drive

During the working process of the cleaning sieve box, the shaft drives the sieve box to reciprocate through an eccentric wheel, and its front bearing moves synchronously along the guide rail. The driving part is coordinated with the guide rail to ensure stable reciprocating motion of the cleaning sieve box. The guide rail components are fixed and installed on the frame with bolts to ensure structural stability and constrain the vibration direction of the sieve box. When the mixed grain material is released from the threshing drum and falls onto the shaking plate, the material gradually spreads and is transported to the rear of the sieve box under the combined action of the fan airflow and the reciprocating vibration of the shaking plate. Subsequently, the materials are sequentially screened through components such as fish scale screens and mesh screens to achieve the separation of grains and miscellaneous materials (*Chen et al.*, 2022).

Establishment of the finite element simulation model

This paper constructs a 1:1 three-dimensional model of the cleaning sieve box based on the actual object. After importing it into ANSYS Workbench, the material of each component is set to Q235 steel, with parameters shown in Table 1. Modal analysis and transient dynamic simulation analysis of the sieve box was carried out. Modal analysis can be used to determine the natural frequency and vibration mode of the cleaning sieve box, providing a basis for its vibration characteristics, fault diagnosis, and structural dynamic characteristics analysis (*Zhang et al., 2022*). Transient dynamic analysis studies the dynamic response of stress changes over time in the cleaning sieve box during operation (*Wang et al., 2023*).

Material properties of the cleaning sieve box

Table 1

Materials	Density / kg/m³	Elastic modulus / GPa	Poisson's Ratio u	Yield strength / MPa	Tensile strength / MPa
Q235	7850	205	0.3	235	370~500

In the modal analysis, to reduce computational costs and ensure key structural characteristics, the model was appropriately simplified: low-stiffness tail screens were removed to more clearly observe the natural frequencies and mode shapes of the screen box; constrained modal analysis was used to set the front bearings and drive shaft as fixed constraints based on actual installation conditions. In transient dynamic analysis, motion pair constraints were set based on assembly relationships, including rotational pair constraints between the drive shaft and the ground, and fixed pair constraints at the guide rails; complex structures such as fish scale screens were simplified into equivalent loads acting on the screen frame connection components; to simplify calculations, the drive shaft were modeled as rigid bodies to neglect their dynamic responses; The drive shaft speed was set to 5 r/s, and the simulation duration was set to 0.2 seconds (time required for one reciprocating vibration) to balance computational efficiency. The corresponding model settings are shown in Fig. 2.

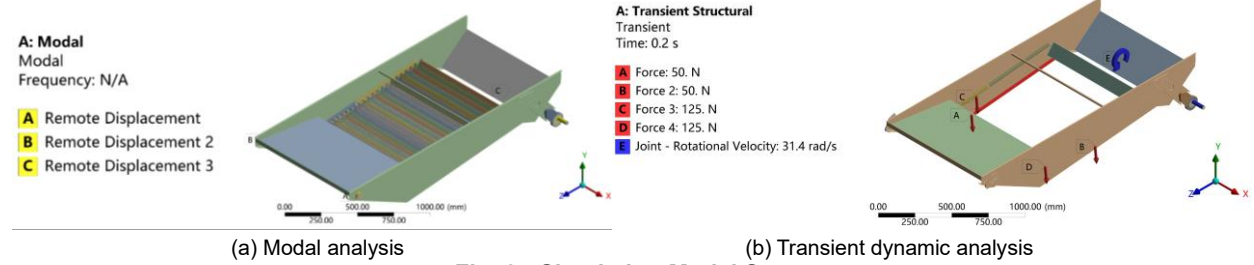


Fig. 2 - Simulation Model Setup

Based on its structural characteristics, the cleaning sieve box model utilized a 6 mm primary mesh size, and was optimized using grid partitioning methods such as patch fitting. The modal analysis model was discretized into 752,068 elements, with a mesh quality of 0.75. The dynamic analysis model was divided into 477,544 elements, with a mesh quality of 0.72. The mesh division results are shown in Fig. 3.

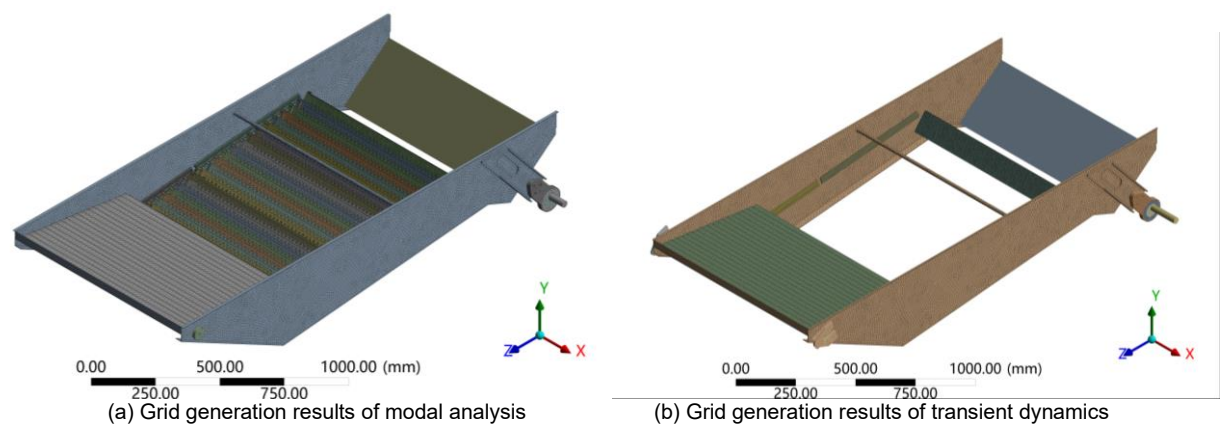


Fig. 3 - Grid generation of the cleaning sieve box

Construction of the test bench for the cleaning sieve box

In response to the difficulties in signal acquisition and severe interference faced by the cleaning sieve box of the combine harvester under complex field conditions, an open cleaning sieve box test bench was designed. The test bench can simulate the actual working state of the sieve box in a controllable environment, providing stable and reproducible test conditions for signal acquisition. The test bench consists of a sieve box, a frequency converter, an electric motor, a front (rear) support base, a test platform, and connecting components. The support base was divided into front and rear supports. The bottom of the front and rear support bases was equipped with U-shaped grooves, which were fixed to the test platform by nuts. The upper end face of the support base was equipped with connection holes. The connecting components and guide rail support plates were fixed and installed on the support base through bolts. The three-dimensional model of the test bench is shown in Fig. 4, and relevant equipment parameters are shown in Table 2.

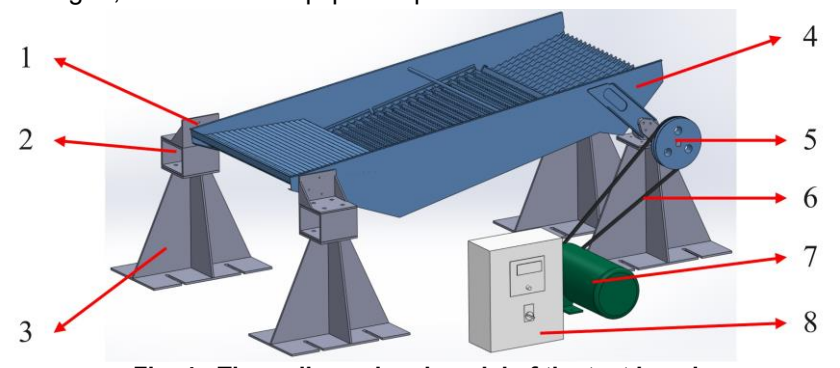


Fig. 4 - Three-dimensional model of the test bench 1-Guide rail support plate; 2-Connecting components; 3-Support base; 4-Cleaning sieve box; 5-Driving; 6-Conveyor belt; 7-Motor; 8-Frequency converter

Main parameters of the test bench for the cleaning sieve box

Table 2

-	-
Items	Parameters
Cleaning sieve box	Length: 2.1 m; Width: 0.91 m
Front support base	Length: 0.65 m; Width: 0.4 m; Height: 0.5 m
Rear support base	Length: 0.7 m; Width: 0.4 m; Height: 0.567 m
Motor	Three-phase electricity 4.0kW-2 level 2800
Frequency converter	Three-phase electrical level 5.5 kW
Gear ratio of the belt pulley	3.125

To simulate the material load on the screening surface of the cleaning sieve box during operation, material bearing bags with shaking plates and fish scale screening surfaces were placed. The weight of the rice placed can be calculated based on the feeding amount and the proportion of the discharged material during grain harvesting (*Liang and Wada, 2023*).

The calculation formula is as follows:

$$m_{out}(t) = m_{in}(t) \cdot \eta_{out}(t) \tag{1}$$

where: $m_{out}(t)$ is the mass flow rate of the ejected material at time t, kg/s; $m_{in}(t)$ is the feed rate at time t,

kg/s, and $\eta_{out}(t)$ is the proportion of threshed material. When the feeding rate was 5 kg/s, the proportion of threshed material was 0.4, and the operating time t was 2 s, the calculated mass of threshed material was 4 kg. In the experiment, rice grains of equal quality were evenly placed in material-bearing bags, as shown in Fig. 5.

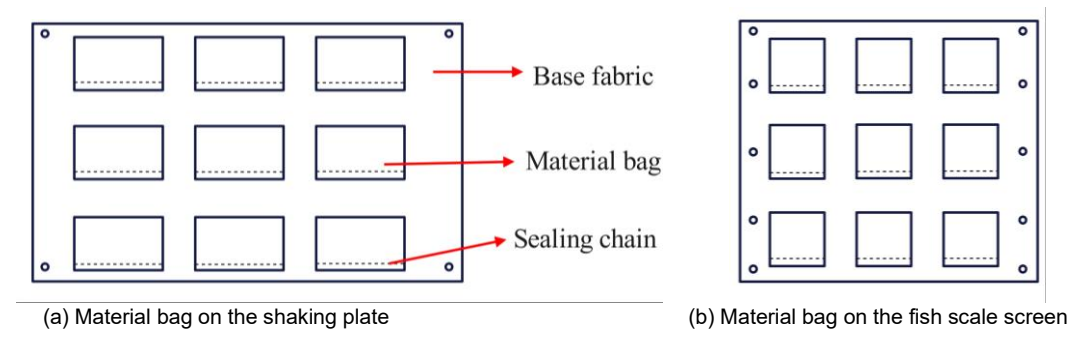


Fig. 5 - Structure of material bag

Based on the above design, the physical test bench for the cleaning sieve box is shown in Fig. 6. The test bench employs a motor-pulley transmission system to provide stable power for the cleaning sieve box, with a pulley transmission ratio of 3.125. During the experiment, the working vibration frequency of the cleaning screen box was set to 5 Hz. The vibration frequency of the sieve box refers to the number of vibration cycles completed per unit time, measured in Hertz (Hz). The relationship between the vibration frequency and the rotational speed of the drive shaft is expressed as follows:

$$f = \frac{n}{60} \tag{2}$$

where f is the vibration frequency (Hz), and n is the rotational speed (r/min).

According to the calculation, the drive shaft speed was determined to be 300 r/min. Based on the pulley transmission ratio, the motor speed was set to 937.5 r/min to ensure that the sieve box operated at the predetermined vibration frequency.



Fig. 6 - Test bench of the cleaning sieve box

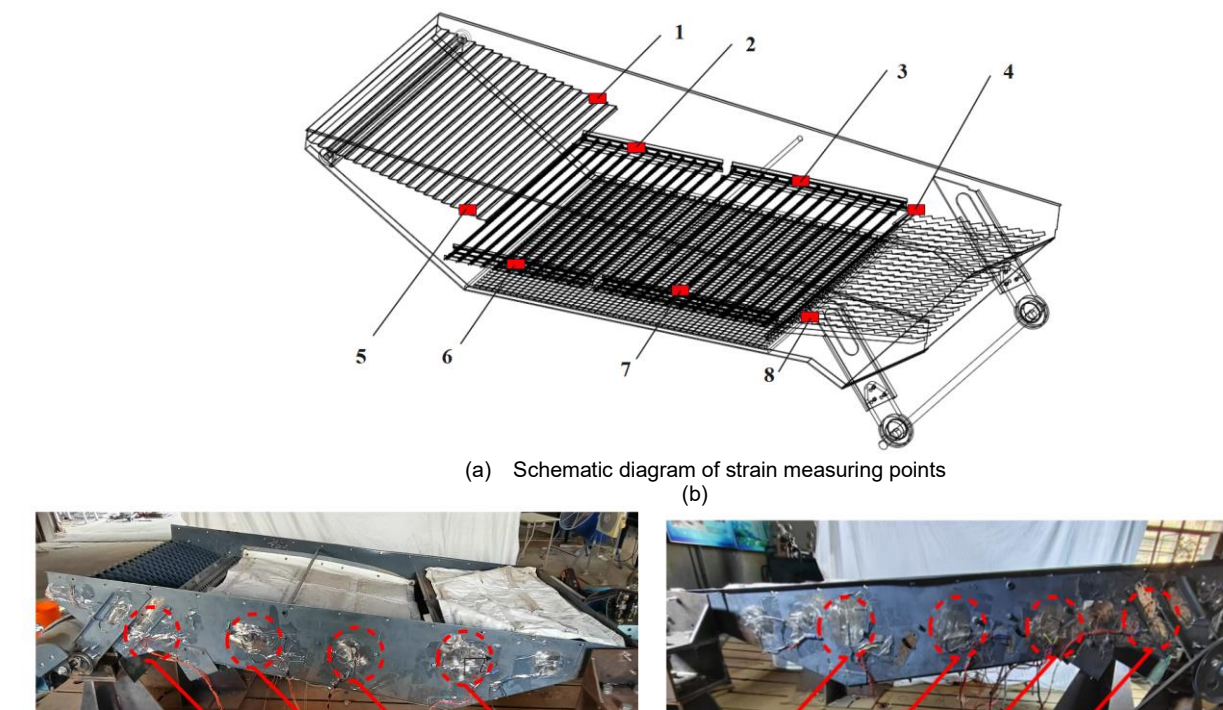
Stress load signal acquisition

To accurately capture the strain load signal of the cleaning sieve box under working condition, a strain data acquisition system was developed, consisting of strain sensors, data acquisition modules, and upper computer software. The strain sensors used were Chengke 120-1AA strain gauges, and the data acquisition module was a Chengke CT9300 dynamic strain signal acquisition instrument. The collected data were transmitted to the upper-computer software for real-time display, storage, and analysis. The experimental setup and equipment are shown in Fig. 7. Prior to the experiment, all strain sensors were calibrated to minimize measurement errors and ensure synchronized data collection for subsequent analysis. To prevent signal aliasing and distortion, the sampling frequency was set to 1000 Hz, allowing accurate acquisition of strain load signals during the stable operation of the cleaning sieve box.



Fig. 7 - Strain data acquisition system

Based on the transient dynamic analysis of the sieve box, several stress concentration zones were identified in the connection areas between the shaking plate, fish-scale screen frame, tail screen plate, and the main screen frame. These regions are highly susceptible to fatigue damage during the reciprocating motion of the sieve box and were therefore selected as strain measurement points to monitor the structural stress state in real time (*Hwang et al., 2024*). Due to the complex geometry of the shaking plate, fish-scale screen, and tail baffle, sensor installation was relatively difficult. Consequently, strain gauges 1 and 5 were placed at the connection between the tail end of the shaking plate and the screen frame. Strain gauges 2 and 6 were positioned at the one-third (1/3) location along the connection between the fish-scale screen frame and the screen frame, while strain gauges 3 and 7 were installed at the two-thirds (2/3) position. Strain gauges 4 and 8 were mounted at the connection between the center of the tail screen and the screen frame. The layout of these measuring points is shown in Fig. 8.



(b) Actual layout of strain measuring points

Fig. 8 - Strain measuring points on the cleaning sieve box

Fatigue life analysis

3

In this study, nCode fatigue analysis software was used to predict the fatigue life of the cleaning sieve box. The analysis was conducted based on the load spectrum obtained using the rainflow counting method, combined with the S–N curve characteristics of the material. The fatigue life was then predicted and evaluated according to Miner's linear cumulative damage theory. The nCode analysis workflow is illustrated in Fig. 9.

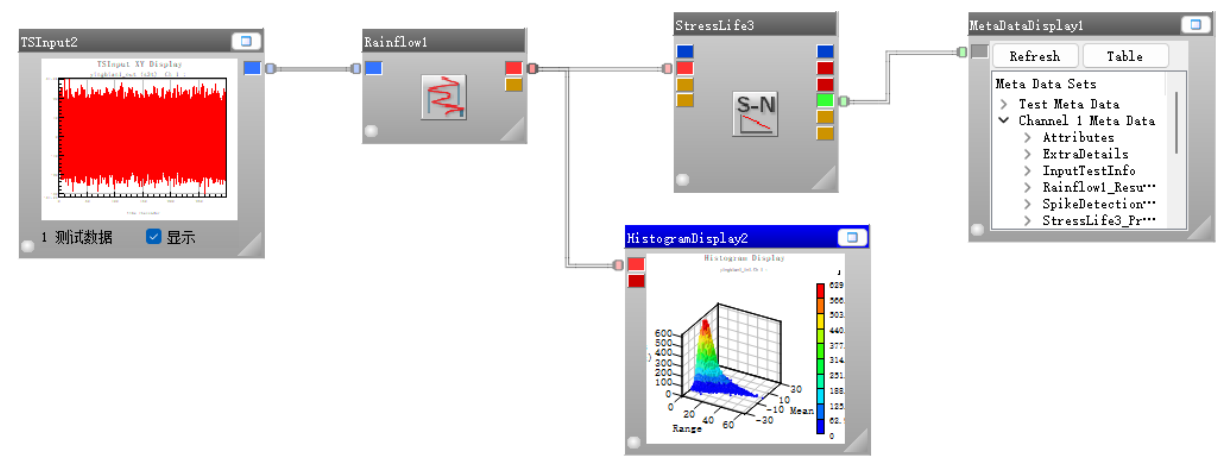


Fig. 9 - Fatigue life analysis process of the cleaning sieve box

During operation, the cleaning sieve box is subjected to variable-amplitude loads. The rainflow counting method was employed to perform cyclic counting of the stress load signals at the measuring points, providing the data foundation for subsequent fatigue life analysis. This method effectively extracts stress cycles from complex load signals. The fatigue life calculation of the sieve box material was conducted using the StressLife module in nCode software, with the relevant parameters configured according to the material's mechanical properties (*Bagni et al., 2024*; *He et al., 2024*). The physical meanings and calculation methods of the corresponding parameters are summarized in Table 3.

Parameters of StressLife module in nCode

Table 3

Parameters	Physical meaning	Numerical size
Ε	Young's modulus	Parameters of the material
UTS	Ultimate tensile strength	Parameters of the material
R	Fatigue testing stress ratio	$\sigma_{ ext{min}}$ / $\sigma_{ ext{max}}$
S1	Stress values under 10 ³ cycles	$0.9 \times UTS$
S2	Stress values under Nc1 cycles	$0.357 \times UTS$
SRI1	Cut-off value for stress range	$2\times S2/(Nc1)^{b1}$
b1	First Fatigue Strength Index	$(\log(S2) - \log(S1) / (\log(Nc1) - 3)$
Nc1	Inflection point value of the fatigue curve	10 ⁶ ~10 ⁷
b2	Second fatigue strength index	b1/(2+b1)

It is worth noting that the load ratio of the sieve box in actual working conditions is not fixed. Therefore, it is necessary to introduce an average stress correction to compensate for the difference between the actual load and the standard fatigue test conditions, thereby ensuring the reliability of the predicted fatigue life of the sieve box (*Kim et al., 2024*). The Goodman correction method was used to adjust the average stress of the sieve box load signal. The calculation formula is expressed as follows:

$$\frac{\sigma_a}{\sigma_e} + \frac{\sigma_m}{\sigma_b} = 1 \tag{3}$$

where σ_a is the fatigue limit under symmetric cyclic loading; σ_m is the mean stress, and σ_b is the ultimate tensile strength of materials.

Subsequently, the Miner fatigue damage theory was applied to obtain the fatigue life results of the sieve box. This theory assumes that fatigue damage at different stress levels accumulates linearly. When the sum of the accumulated damage values reaches 1, the material experiences fatigue failure, marking the end of its fatigue life. The calculation formula is expressed as follows:

$$D = \sum_{i=1}^{m} \frac{n_i}{N_i} \tag{4}$$

where D is the total fatigue damage; m is the number of stress levels S; n_i represents the number of cycles at stress level S_i , N_i represents the total number of cycles of material failure at stress level S_i . When the total damage D is greater than 1, it indicates that the component has failed due to fatigue.

RESULTS AND DISCUSSION Modal analysis

During operation, the cleaning sieve box is subjected to excitation from other parts of the combine harvester. When the excitation frequency approaches the natural frequency of the cleaning sieve box, resonance may occur, resulting in significant structural deformation. Low-order modes are extremely important for evaluating the dynamic stability of structures and predicting its fatigue life. In contrast, high-order modes typically require greater external excitations due to their higher natural frequencies. Their impact on the overall performance of the structure is relatively limited (*Kim et al., 2024*). Accordingly, the first six vibration modes of the sieve box were selected for analysis. The corresponding natural frequencies and mode shapes are presented in Table 4 and illustrated in Fig. 10, respectively.

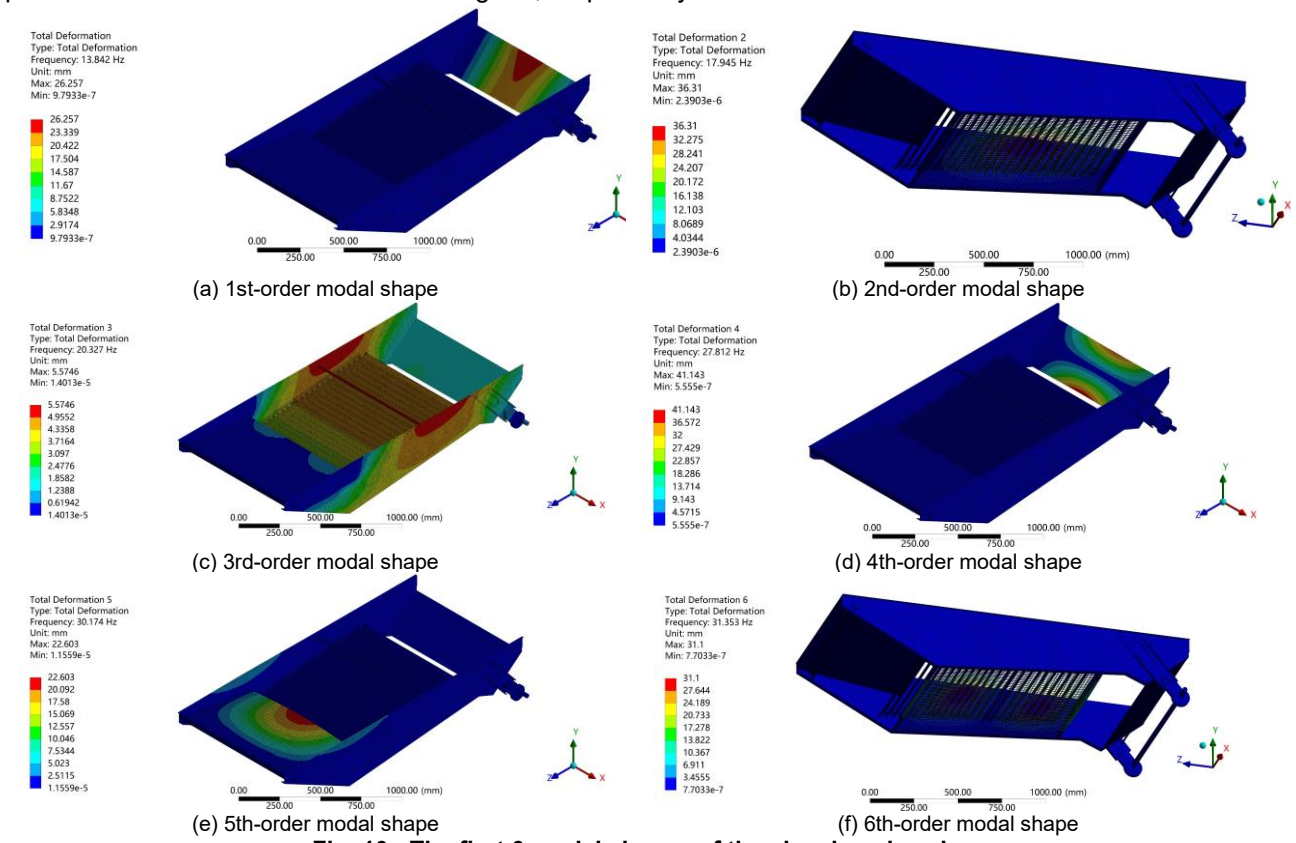


Fig. 10 - The first 6 modal shapes of the cleaning sieve box

Table 4

The first 6 natural frequencies and vibration modes of the cleaning sieve box

Orders	Natural frequencies /Hz	Vibration modes
1	13.842	Lateral bending deformation of tail screen baffle
2	17.945	Horizontal bending deformation of sieve box mesh screen
3	20.327	Twisted deformation in the middle of the sieve box
4	27.812	Lateral bending deformation of tail screen baffle
5	30.174	Bending deformation of shaking plate and screen frame
6	31.353	Twisted deformation of mesh screen

The excitation frequency for the reciprocating motion of the cleaning sieve box during actual operation ranges from 4 to 6 Hz. The first six mode shapes indicate significant vibrational deformation in the middle of the screen frame, the mesh screen, and the tail screen baffle. Modal analysis results indicate that the natural frequencies of the sieve box range from 13.842 to 31.353 Hz. Since the excitation frequency is well separated from the natural frequency range, resonance will not occur, thereby satisfying the operational stability requirements.

Transient dynamics analysis

Fig.11 shows the overall maximum stress time-history in the dynamic analysis of the cleaning sieve box. The stress of the sieve box fluctuates greatly at certain moments, but its overall maximum stress (198.76 MPa) is lower than the tensile strength of the material. This indicates that the stress level of the sieve box during operation is in a safe range, which can ensure that the sieve box maintains a certain safety and stability in long-term operation.

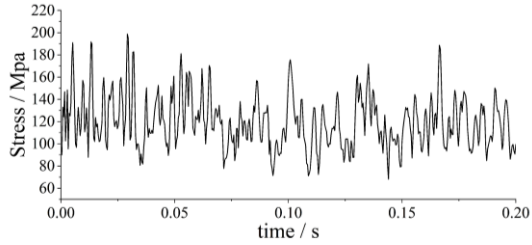


Fig. 11 - Time-history of the maximum overall stress during the operation of the cleaning sieve box

The stress distribution nephogram of the cleaning sieve box at the front and rear positions of the guide rail is shown in Fig.12. The stress distribution on both side frames of the sieve box is highly consistent. The maximum stress values at the front and rear ends of the guide rail are 139.55 MPa and 77.73 MPa, respectively, with both stresses concentrated in the tail sieve and tail sieve baffle regions. Several stress concentration zones were observed at the connections between the sidewalls of the sieve frame and the shaking plate, fish-scale sieve frame, and tail sieve plate, where stress levels ranged from 10 to 50 MPa, significantly higher than those in other regions. This phenomenon is primarily attributed to the combined effects of material loading and structural self-weight during the motion of the cleaning sieve box.

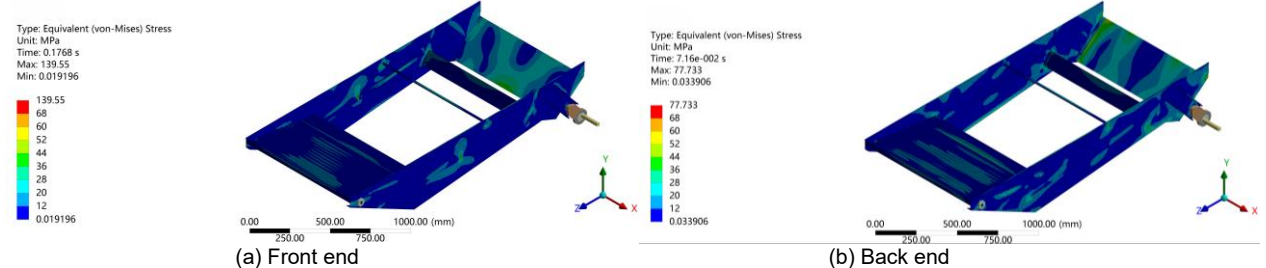


Fig. 12 - Stress distribution of sieve box under normal installation

Results of stress measurement

Through the bench test on the sieve box, the strain load signals of 8 measuring points in the sieve box were obtained. Due to the large number of strain data, 300 seconds of data from each measuring point were selected for analysis. According to Hooke's Law, there is a linear relationship between stress (σ) and strain (ε). In the elastic range of a material, the stress is proportional to strain, expressed as:

$$\sigma = \varepsilon E \tag{5}$$

where E represents the elastic modulus.

The measured strain load signals were converted into stress load signals using this relationship to reflect the stress variation of the cleaning sieve box during operation. Considering the symmetrical installation of the strain sensors, the stress load signals from measuring points 1 to 4 are shown in Fig. 13.

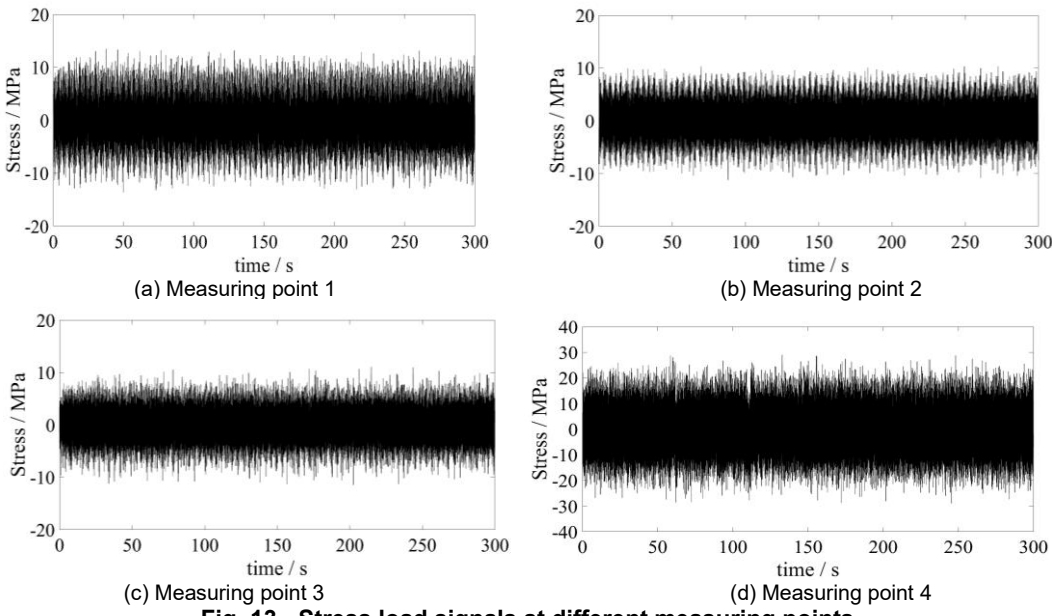


Fig. 13 - Stress load signals at different measuring points

Table 5

Time-domain analysis was conducted on the load signal to determine key features in the stress time history, such as maximum and minimum values. The results are presented in Table 5. The highest stress values were observed at the sensor positions of strain gauges 4 and 8, primarily due to the disturbance and vibration of the tail screen during the operation of the cleaning sieve box. Because of the significant load and stress concentration in this region, special attention should be given to the fatigue life of the connection area.

Characteristics of stress load signals at each measuring point of the sieve box

onaracteristics of stress load signals at each measuring point of the sieve box			
Measuring points	Maximum values / MPa	Minimum values/ MPa	Standard deviation
Sensor 1	13.48	-12.74	3.39
Sensor 2	10.35	-10.26	2.71
Sensor 3	11.08	10.57	2.32
Sensor 4	28.98	-28.92	6.51
Sensor 5	15.02	14.65	3.17
Sensor 6	13.98	11.15	2.77
Sensor 7	12.74	12.24	2.45
Sensor 8	30.58	29.55	7.29

Analysis results of fatigue life of the cleaning sieve box

Rainflow counting analysis was performed on the stress time-history of each measuring point on the sieve box. Due to the symmetrical arrangement of the strain sensor installation positions, only the rainflow counting results for measuring points 1 to 4 are presented in this paper, as shown in Fig. 13. It can be observed from the figure that measuring point 4 exhibits higher stress amplitude compared to other points, indicating that the connection area between the rear sieve and the sieve frame experiences greater loading during operation, making it a critical region for structural fatigue life.

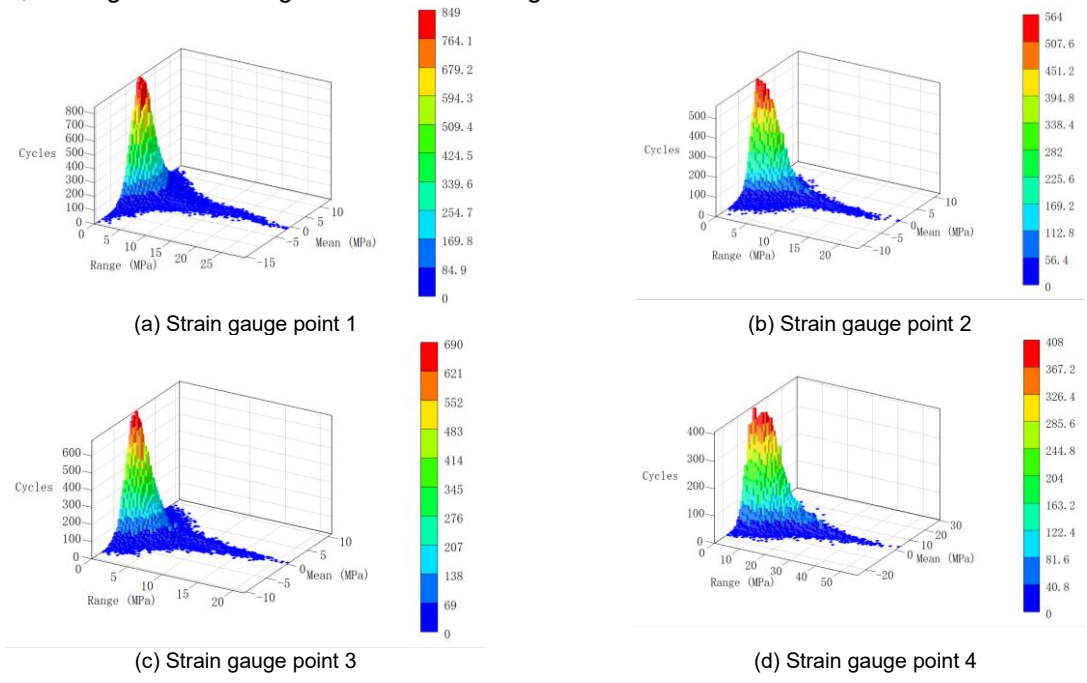


Fig. 13 - Rainflow counting results at different measuring points

Based on the stress-load data measured from the cleaning sieve box, a load spectrum was compiled using the rainflow counting method, and the fatigue life of each measuring point was evaluated using Miner's linear cumulative damage theory. The results are shown in Table 6. The analysis reveals differences in fatigue life among the measuring points, reflecting an uneven load distribution across different parts of the sieve box. The fatigue life at all measuring points exceeded 1×10⁶ cycles, indicating that the overall structure possesses good fatigue durability and can meet long-term operational requirements. Notably, the fatigue lives at measuring points 4 and 8 were significantly lower, with point 8 exhibiting the shortest life, making it a critical weak area for potential fatigue failure in the sieve box. This can be attributed to two main factors: first, its location at the connection between the tail sieve and the screen frame subjects it to impact during the operation of the tail sieve blades; second, its proximity to the drive motor means that vibrations from power transmission further exacerbate fatigue damage in this area

Table 6

Fatigue life at each measuring point of the cleaning sieve box

Measuring points	Fatigue life (Cycle repeats)	Fatigue damage value
1	1.326×10 ⁸	7.541×10 ⁻⁹
2	3.831×10 ⁸	2.611×10 ⁻⁹
3	3.358×10 ⁸	2.978×10 ⁻⁹
4	5.829×10 ⁶	5.591×10 ⁻⁷
5	1.561×10 ⁶	6.409×10 ⁻⁹
6	2.710×10 ⁸	3.681×10 ⁻⁹
7	3.131×10 ⁸	3.194×10 ⁻⁹
8	5.591×10 ⁶	1.768×10 ⁻⁷

CONCLUSIONS

A fatigue durability test and analysis method for the cleaning sieve box of a combine harvester based on a test bench was proposed to address the issue of fatigue durability during the operation of the cleaning sieve box. Through simulating and analyzing the optimal monitoring position of the strain sensor in the sieve box, its fatigue durability was studied through bench tests. Main conclusions are drawn as follows:

- (1) A finite element model of the cleaning sieve box was established. Modal analysis revealed significant vibrational deformation in the shaking plate, screen frame sidewall, and rear baffle across the first six modes, with the lowest natural frequency of 13.842 Hz. This value substantially exceeds the driving frequency range of the cleaning sieve box (4-6 Hz), effectively eliminating the risk of resonance. Dynamic analysis further identified multiple stress concentration areas at the connections between the shaking plate, fish-scale screen, tail screen, and the screen frame. These regions are prone to fatigue damage during operation and require focused monitoring.
- (2) Through establishing a test bench for the cleaning sieve box, the stress time-history of key measuring points was collected, and the fatigue life of the sieve box was analyzed. The load spectrum of the measured stress load signal was compiled using the rainflow counting method, and the fatigue life evaluation of each measuring point in the sieve box was carried out by combining Miner's linear fatigue cumulative damage theory. The experimental results showed that the structures such as the shaking plate of the cleaning sieve box bore relatively low stress, and their fatigue life was relatively long. In contrast, the fatigue life of the connection area between the screen frame and tail screen was the smallest. This indicates that this area is a potential fatigue weak point in the sieve box structure and needs to be given special attention in structural design and optimization of working condition.

ACKNOWLEDGEMENT

This research was financially supported by National Natural Science Foundation of China (52375249).

REFERENCES

- [1] Bagni, C., Halfpenny, A., Hill, M., & Tarasek, A. (2024). A practical methodology for the fatigue life estimation of adhesive joints. *Procedia Structural Integrity*, *Vol.* 57, pp. 598-610. https://doi.org/10.1016/j.prostr.2024.03.066
- [2] Chen, X., He, X., Wang, W., Qu, Z., & Liu, Y. (2022). Study on the technologies of loss reduction in wheat mechanization harvesting. *Agriculture*, *Vol.* 12(11), 1935. https://doi.org/10.3390/agriculture12111935
- [3] Doungpueng, K., Saengprachatanarug, K., Posom, J., & Chuan-Udom, S. (2020). Selection of proper combine harvesters to field conditions by an effective field capacity prediction model. *International journal of agricultural and biological engineering*, *Vol.* 13(4), pp. 125-134. https://doi.org/10.25165/j.ijabe.20201304.4984
- [4] He, J., Wang, Z., Gao, B., Yu, D., Ma, Y., Zhong, W., & Wang, J. (2024). Fatigue Analysis of PTO Gearboxes in Paddy Power Chassis Using Measured Loads. *Agriculture*, *Vol.* 14(9), 1436. https://doi.org/10.3390/agriculture14091436
- [5] Hwang, I. S., Kim, J. H., Im, W. T., Jeung, H. H., Nam, J. S., & Shin, C. S. (2024). Analyzing Safety Factors and Predicting Fatigue Life of Weak Points in an Electrically Driven, Multi-Purpose Cultivation Tractor. *Agriculture*, Vol. 14(3), 416. https://doi.org/10.3390/agriculture14030416

- [6] Jin, M., Zhao, Z., Chen, S., & Chen, J. (2022). Improved piezoelectric grain cleaning loss sensor based on adaptive neuro-fuzzy inference system. *Precision Agriculture*, *Vol.* 23(4), pp. 1174-1188. https://doi.org/10.1007/s11119-022-09879-2
- [7] Kim, J. H., Gim, D. H., & Nam, J. S. (2024). Experimental Structural Safety Analysis of Front-End Loader of Agricultural Tractor. *Agriculture*, *Vol.* 14(6), 947. https://doi.org/10.3390/agriculture14060947
- [8] Li, Y., Pang, J., Xu, L., Tang, Z., & Zhou, Y. (2019). Manufacturing defect location of cleaning sieve in grain combine harvester based on vibration excitation source tracing (基于振动激励溯源的谷物联合收获机清选筛制造缺陷定位). *Transactions of the Chinese Society of Agricultural Engineering*, *Vol.* 35(5), pp. 10-17. https://doi.org/10.11975/j.issn.1002-6819.2019.05.002 (in China)
- [9] Liang, Z., & Wada, M. E. (2023). Development of cleaning systems for combine harvesters. *Biosystems Engineering*, *Vol.* 236, pp. 79-102. https://doi.org/10.1016/j.biosystemseng.2023.10.018
- [10] Linhares, T. B., & Vimieiro, C. B. S. (2024). Evaluation of the movement performance of a vibrating screen due to machining errors on the shaft. Engineering Failure Analysis, Vol. 161, 108260. https://doi.org/10.1016/j.engfailanal.2024.108260
- [11] Linhares, T. B., da Silva Scari, A., & Vimieiro, C. B. S. (2024). Causes of failures in vibrating screens: a literature review. *Minerals Engineering*, *Vol. 218*, 109027. https://doi.org/10.1016/j.mineng.2024.109027
- [12] Mirzazadeh, A., Abdollahpour, S., & Hakimzadeh, M. (2022). Optimized Mathematical Model of a Grain Cleaning System Functioning in a Combine Harvester using Response Surface Methodology. *Acta Technol. Agric*, *Vol.* 25, pp. 20-26. https://doi.org/10.2478/ata-2022-0004
- [13] Pang, J., Lin, Y., Wang, S., Du, Z., Xie, L., & Chen, X. (2023). Vibration analysis and structural optimization of grain cleaning sieve based on VMD (基于优化 VMD 的谷物清选筛振动分析与结构优化). *Transactions of the Chinese Society of Agricultural Engineering*, *Vol.* 39(12), pp. 1-9. https://doi.org/10.11975/j.issn.1002-6819.202303082 (in China)
- [14] Ramatsetse, B., Mpofu, K., & Makinde, O. (2017). Failure and sensitivity analysis of a reconfigurable vibrating screen using finite element analysis. *Case studies in engineering failure analysis*, *Vol.* 9, pp. 40-51. https://doi.org/10.1016/j.csefa.2017.04.001
- [15] Rumiche, F., Noriega, A., Lean, P., & Fosca, C. (2021). Metallurgical failure analysis of a welded drive beam of a vibrating screen. *Engineering Failure Analysis*, *Vol. 118*, 104936. https://doi.org/10.1016/j.engfailanal.2020.104936
- [16] Wang, L., Zhang, S., Cui, T., Gao, Y., & Wang, B. (2023). Kinetic characteristics of a bionic screen with continuous variable amplitude from front to rear and behaviour of maize mixture on the screen. *Powder Technology*, Vol. 424, 118370. https://doi.org/10.1016/j.powtec.2023.118370
- [17] Wang, L., Zhang, X., Leng, J., Zhao, G., Jiao, Z., & Qin, Y. (2018). Fatigue life analysis of cleaning device in grain combine harvester (谷物联合收获机清选装置疲劳寿命分析). *Journal of Agricultural Machinery*, *Vol. 49*(S1), pp. 282-287. https://doi.org/10.6041/j.issn.1000-1298.2018.S0.037 (in China)
- [18] Yang, L., Yaoming, L., Liya, L., & Maolin, S. (2024). Modeling and control methods of a multi-parameter system for threshing and cleaning in grain combine harvesters. *Computers and Electronics in Agriculture*, *Vol. 225*, 109251. https://doi.org/10.1016/j.compag.2024.109251
- [19] Zhang, C., Mousavi, A. A., Masri, S. F., Gholipour, G., Yan, K., & Li, X. (2022). Vibration feature extraction using signal processing techniques for structural health monitoring: A review. *Mechanical Systems and Signal Processing*, Vol. 177, 109175. https://doi.org/10.1016/j.ymssp.2022.109175